Pergamon

0022-4073(94)00122-7

J. Quant. Spectrosc. Radiat. Transfer Vol. 53, No. 3, pp. 335–346, 1995

0022-4073/95 $9.50 + 0.00

CORRELATED-k FICTITIOUS GAS MODEL FOR H_2O INFRARED RADIATION IN THE VOIGT REGIME

PH. RIVIÈRE, A. SOUFIANI, and J. TAINE†

Laboratoire d'Energétique Moléculaire et Macroscopique, Combustion du CNRS et de l'ECP, École Centrale Paris, Grande Voie des Vignes, 92295 Châtenay-Malabry, France

(Received 10 March 1994; received for publication 30 December 1994)

Abstract—The ability of the correlated-k fictitious gas (ckfg) approach to accurately predict radiative transfer in strongly nonhomogeneous media is studied for the case of water vapor absorption lines with Voigt profiles. In the ckfg approach, the real gas is considered as a mixture of fictitious gases, each one characterized by absorption lines with similar transition lower level energies. The correlated-k approach is then applied to each gas and the spectra of different gases are assumed to be uncorrelated. The model is studied for a range of temperatures (180–2500 K) and pressures (10^{-2} atm). In addition, the model takes into account the nonlorentzian behavior of the far wings. The model parameters are obtained from line-by-line calculations based on approximate spectroscopic data suitable for high temperature and low spectral resolution applications. The choice of the quadrature for spectral integrations and of the lower level energy E'' ranges is discussed. ckfg results are compared to the reference line-by-line calculations and to the results from the correlated-k (ck) approach, and from available statistical narrow-band (SNB) models in the Voigt regime. It is shown that a 10 point quadrature may be sufficiently accurate, even for very small line widths. ckfg results agree well with line-by-line calculations while ck and SNB models may strongly underestimate the intensity of radiation emitted by a hot gaseous column and transmitted through a long cold column.

1. INTRODUCTION

Radiative transfer in water vapor at pressure lower than 10^{-1} atm is important in the fields of combustion, atmospheric physics, and long range sensing. For such pressures and for temperatures in the range [180–2500 K], water vapor absorption lines are characterized by the Dicke–Galatry profile.[1,2] If the collisional broadening and the Doppler broadening have the same order of magnitude, the Dicke–Galatry profile can be approximated by a Voigt profile with a local maximum error in the absorption coefficient of about 20%.[3] In fact, the use of a Dicke–Galatry or a Voigt profile is sufficiently accurate near line centers for the calculations of low resolution spectra (about 10 cm^{-1}). But both the Dicke–Galatry and Voigt profiles are inadequate in the far line wings, for which they tend towards lorentzian behavior and take into account neither the finite duration of collisions nor the line coupling effects. It is necessary to consider the deviations from the Lorentz line shape when the contribution of far line wings to absorption is not negligible, i.e., for long atmospheric paths. Many authors[4–7] have theoretically modelled the phenomena leading to these deviations. More empirically, multiplicative functions, called χ functions, which modify the absorption coefficient in the far line wings have been adjusted by Clough et al[8] to fit the experimental spectra of Burch et al[9–11] for self- and *air*-broadening of H_2O lines at atmospheric temperatures, and by Hartmann et al[7] for pure water vapor up to 800 K.

The precise calculation of H_2O absorption spectra for the above-mentined temperature and pressure conditions requires a spectral resolution better than 10^{-3} cm^{-1}. The use of such a high resolution in practical applications involving the resolution of the radiative transfer equation in a large spectral range would require very long CPU times. A low resolution modelling of radiative properties (25 cm^{-1} typically) is then desirable. In the Lorentz regime, Statistical Narrow-Band

†To whom all correspondence should be addressed.

(SNB) models yield simple analytical expressions of the transmissivity of a homogeneous column, averaged over each narrow band.[3,12] These functions depend generally on few parameters tabulated as a function of temperature and wave-number.[13–18] The extension of SNB models to nonuniform paths requires further approximations, such as those by Curtis–Godson or Lindquist–Simmons studied by Young.[19]

SNB models have also been formulated for the Doppler regime for both uniform[20] and nonuniform paths.[21,22] For the Voigt regime, only a regular narrow-band rigorous approach has been developed,[23] but no simple expression of the mean transmissivity has been obtained. Nevertheless, different approximations have been used to extend SNB models to the Voigt case: (i) In a first type of approximation, the Voigt profile is replaced by a rectangular[24] or a parabolic[25] profile near the line center and by lorentzian wings in order to obtain simple analytical expressions of the mean transmissivity using an analysis similar to that used in the lorentzian case. (ii) In a second type of approximation, the mean transmissivity is approximated analytically from the mean transmissivities calculated for both the Lorentz and Doppler profiles.[26–29] On the other hand, the far wing nonlorentzian behavior has been taken into account in a statistical narrow-band model developed for the Lorentz regime.[30] For nonuniform paths, Curtis–Godson and Lindquist–Simmons approximations, which introduce additional errors in the Lorentz regime, especially in teledetection applications, have never been checked to our knowledge for the more general Voigt profile or for the Doppler profile.

The use of the correlated k-distribution function (ck) is another approach to low resolution radiative property modelling. The actual absorption spectrum is replaced by the absorption spectrum reordered by increasing absorption coefficient values. Indeed, the reordered spectrum corresponds to the reciprocal of the cumulative distribution function of the absorption coefficient inside a narrow-band, which is a monotonic function. Accurate integration of this function requires only few points. This model is widely used in the field of atmospheric physics[31–35] and thus for the Voigt profile. It allows a description of radiative properties in terms of absorption coefficients rather than mean transmissivities. Nevertheless, it is inadequate for the treatment of long-range detection of hot gas emission.[36]

The correlated-k fictitious gas model (ckfg)[36,37] is an extension of the ck approach to strongly nonisothermal media. In a previous paper, we have developed and analyzed this model in the Lorentz regime for H_2O near 2.7 μm.[36] It was shown to be much more accurate than ck and SNB models for applications involving long range sensing of emission by hot gases.

The aim of the present work is to develop and analyse the ck and ckfg models in the more general Voigt regime for all H_2O i.r. bands. More precisely, the accuracies of ck and ckfg models are studied over the temperature and pressure ranges (180–2500 K) and (10^{-2}–6 atm) respectively. The parameters of the models have been obtained from line-by-line calculations using the approximate spectroscopic high temperature data bases of Ref. 38. The far wings of the Voigt profile are corrected by using the χ functions of Ref. 8 for large atmospheric paths at low temperatures. The principles of ck and ckfg models are briefly summarized and their practical implementation (i.e., the choice of the quadrature and of energy classes) is discussed in Sec. 2 for H_2O–air mixtures. Some commonly used SNB models suitable for the Voigt regime are also briefly presented in this section. In Sec. 3, the quality of the ckfg model is tested against the line-by-line approach, considered as a reference, and is compared to the qualities of the other approximate ck and SNB models. More precisely, we compare in this section the low resolution radiative properties of homogeneous and nonhomogeneous columns and the radiative intensities emitted by these columns.

2. ck, ckfg AND SNB MODELS IN THE VOIGT REGIME

2.1. ck and ckfg models

The ck approach is based on the cumulative distribution function $g^{\Delta\nu}(k, r)$ of the spectral absorption coefficient $\kappa_\nu(r)$ in each narrow band interval, $\Delta\nu$, at each point r of the medium.[3] $g^{\Delta\nu}(k, r)$ is the fraction of $\Delta\nu$ where the associated absorption coefficient $\kappa_\nu(r)$

is less than the prescribed value k. The transmissivity averaged over $\Delta\nu$ of a column of length l is then

$$\bar{\tau}^{\Delta\nu} = \frac{1}{\Delta\nu}\int_{\Delta\nu} \exp\left[-\int_0^l \kappa_\nu(s)\,\mathrm{d}s\right]\mathrm{d}\nu \tag{1}$$

$$\bar{\tau}^{\Delta\nu} = \int_0^1 \exp\left[-\int_0^l k_g(s)\,\mathrm{d}s\right]\mathrm{d}g, \tag{2}$$

where s is the spatial coordinate along the column and the function $g \to k_g(s)$ is the reciprocal of the function $k \to g^{\Delta\nu}(k, s)$. The use of Eq. (2) instead of Eq. (1) enables a very large reduction in computational time, since the function $k \to g^{\Delta\nu}(k, s)$ varies monotonically and much more smoothly than does the function $\nu \to \kappa_\nu(s)$. However, the ck model is not accurate for strongly nonisothermal media.[36] In fact, for a given narrow-band, it is assumed in this model that the wave-number corresponding to the maximum emission from a hot medium is equal to the wave-number corresponding to the maximum absorption by a cold medium. This assumption does not take into account the different variations with temperature of the line intensities characterized by different lower level energies, E''.

In the ckfg model the real gas is considered as a mixture of N fictitious gases, each characterized by the absorption lines of the real gas whose lower level energies, E'', belong to a given range. This energy range must be sufficiently narrow so that the ck method yields accurate results when applied to each fictitious gas, even for strongly nonisothermal media. The spectra of different fictitious gases are assumed to be uncorrelated. This leads to

$$\bar{\tau}^{\Delta\nu} = \prod_{j=1}^{N}\int_0^1 \exp\left[-\int_0^l k_g^j(s)\,\mathrm{d}s\right]\mathrm{d}g, \tag{3}$$

where $k_g^j(s)$ is the inverse of the cumulative distribution function of the absorption coefficient associated with the jth fictitious gas at point s.

The choice of each E'' range, which defines a fictitious gas, results then from two opposing considerations: (i) The accuracy of the ck method applied to a fictitious gas increases when the width of the E'' range decreases. In fact, the ratio of the intensities of two significant lines must not vary from a value much higher than 1 at a given temperature to a value much smaller than 1 at another temperature. (ii) When the number of ranges increases, the number of lines for each fictitious gas decreases and thus the variations of the function $g \to k_g^j(s)$ become steeper. Hence, increasing the number of ranges leads to an increase in computational times since both the number of ck calculations and the number of required integration points increase.

In practice, the number of E'' ranges has been arbitrarily chosen equal to five. The five fictitious gases lead to similar amounts of emission at 2500 K, which is the maximum temperature considered here. More precisely, we introduce the function

$$F(E'', T) = \sum_{\substack{\text{line } i \\ E_i'' \leqslant E''}} S(i, T), \tag{4}$$

where $S(i, T)$ is the intensity at temperature T of a line i characterized by the lower level energy E_i''. Figure 1 shows the ratio

$$\mathscr{R}(E'') = \frac{F(E'', 2500\ \mathrm{K})}{F(\infty, 2500\ \mathrm{K})} \tag{5}$$

vs E''. The values $E'' = 1500$, 3000, 4500, and 6500 cm^{-1} are chosen to define the boundaries of the classes associated with the five fictitious gases and correspond respectively to $\mathscr{R}(E'') = 0.1$, 0.27, 0.46, and 0.68. In fact, the widths of the E'' ranges increase with E'' in order to increase the accuracy for colder media.

The spectral integration in terms of the variable g is carried out by using a N_q point quadrature

$$\bar{\tau}^{\Delta\nu} = \prod_{j=1}^{N}\sum_{m=1}^{N_q} \omega_m \exp\left[-\int_0^l k_{g_m}^j(s)\,\mathrm{d}s\right], \tag{6}$$

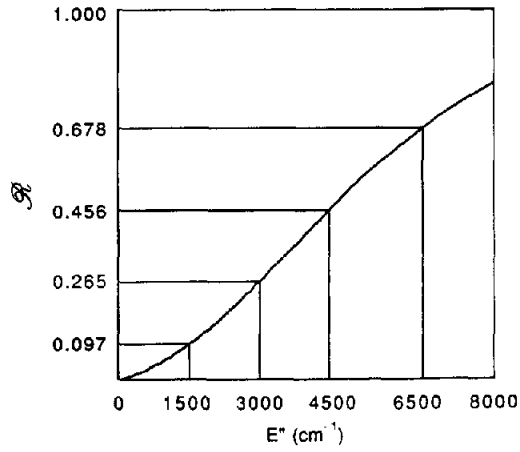

Fig. 1. Normalized distribution of line intensities at 2500 K [Eqs. (4) (5)] vs the energy of the transition lower level.

where g_m and ω_m are the points and the weights of the quadrature, respectively. It has been shown that a seven point quadrature yields accurate results for water vapor in the Lorentz line shape regime and at pressures higher than 10^{-1} atm.[36] For lower pressures and Voigt line shapes, we have studied the accuracy of the two quadratures characterized by 10 and 17 points, given in Table 1. To this end, we have computed the emissivity averaged over the spectral range $[0, \Delta\nu]$ of an isolated Voigt line, centered on one boundary of the spectral range and characterized by the collisional, γ_L, and Doppler, γ_D, half-widths at half-height, for different values of $\gamma_L/\Delta\nu$ and $\gamma_D/\Delta\nu$. By varying these ratios we simulate the effect of a varying number of lines on the reordered absorption coefficient inside $\Delta\nu$. Figures 2 and 3 show the relative errors in the averaged emissivity introduced by the use of the 10 and 17 point quadratures, respectively, as a function of the averaged emissivity, which depends on the column length or the line intensity. Error variations are very different in the cases of Lorentz and Doppler lines. The monochromatic emissivity in the case of a Doppler line shows a steep variation near a wave-number which varies with the Doppler width or the column length. These variations introduce sharp peaks in the quadrature discrepancies, which do not appear for Lorentz profiles. Except for the case corresponding to very low pressures characterized by $\gamma_L/\Delta\nu = 10^{-7}$, the errors are lower than 40 and 2% for an emissivity greater than 10^{-3}, for the 10 point and the 17 point quadratures, respectively. These errors become respectively 8 and 2%

Table 1. ω_m and g_m are the weights and points of the 10 and 17 point quadratures used for spectral integrations in ck and ckfg models.

m	17 points		10 points	
	g_m	ω_m	g_m	ω_m
1	0.00000000	0.450000E-1	0.00000000	0.07500000
2	0.15540585	0.245000E+0	0.24875388	0.37500000
3	0.45000000	0.320000E+0	0.65124612	0.37500000
4	0.74459415	0.245000E+0	0.90000000	0.09000000
5	0.90000000	0.495000E-1	0.94500000	0.06000000
6	0.91554058	0.245000E-1	0.99000000	0.01650000
7	0.94500000	0.320000E-1	0.99450000	0.00600000
8	0.97445942	0.245000E-1	0.99900000	0.00166667
9	0.99000000	0.495000E-2	0.99950000	0.00066667
10	0.99155406	0.245000E-2	1.00000000	0.00016667
11	0.99450000	0.320000E-2		
12	0.99744594	0.245000E-2		
13	0.99900000	0.500000E-3		
14	0.99917267	0.272222E-3		
15	0.99950000	0.355556E-3		
16	0.99982733	0.272222E-3		
17	1.00000000	0.500000E-4		

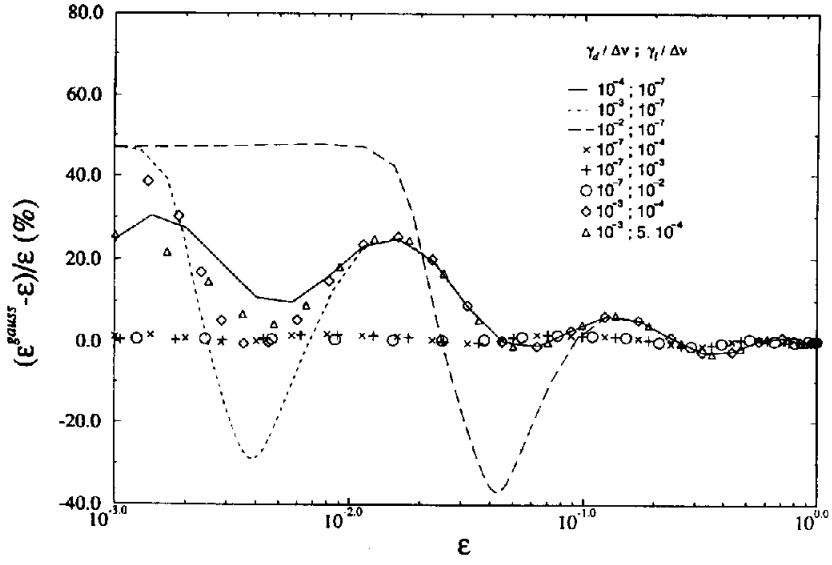

Fig. 2. Accuracy of the 10 point quadrature of Table 1: relative error in the emissivity averaged over $\Delta\nu$ of an isolated Voigt line centered on one boundary of $\Delta\nu$ for various Lorentz and Doppler half-widths.

for mean emissivities greater than 0.03. In fact, it is shown in Sec. 3 that, for real spectra and pressures higher than 0.1 atm, the 10 point quadrature is sufficiently accurate.

Model parameters for a given spectral band are the reordered absorption coefficients k^j_{gm}, where j designates the fictitious gas (j varies from 1 to 5 for the five gas ckfg model and $j = 1$ for the ck model) and m is the quadrature point. The spectrum is divided into 25 cm^{-1} wide bands whose center locations are 150, 175, ..., cm^{-1} in order to enable comparisons with SNB calculations. The parameters k^j_{gm} have been obtained for various conditions of pressure, p, and temperature, T, by reordering the results of line-by-line calculations. These calculations use the approximate spectroscopic data base described in the Ref. 38. We use the rotationally-dependent collisional broadening coefficients of Ref. 39 and the Voigt profile is computed using the algorithm of Ref. 40. The far line-wings have been corrected below 300 K by using the empirical χ functions of Ref. 8:

$$\chi = \begin{cases} 1-(1-\chi')[(\nu-\nu_i)/25]^2, & |\nu-\nu_i| \leqslant 25\ \text{cm}^{-1} \\ \chi', & |\nu-\nu_i| \geqslant 25\ \text{cm}^{-1}, \end{cases} \tag{7}$$

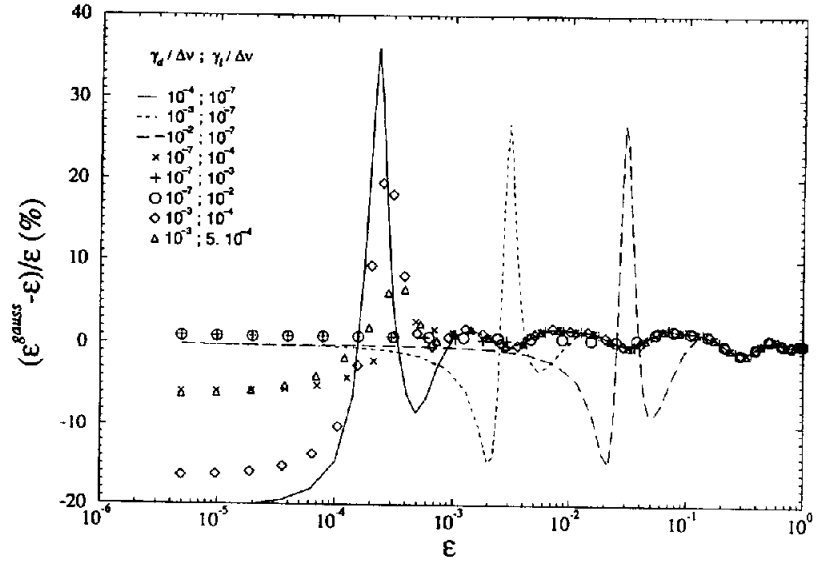

Fig. 3. Same as in Fig. 2 for the 17 point quadrature of Table 1.

where ν_i is the line center position and χ' is given for self-broadening by

$$\chi' = 8.63 \exp\left[-\left(\frac{\nu-\nu_i}{400}\right)^2\right] + \left[0.83\left(\frac{\nu-\nu_i}{250}\right)^2 + 0.033\left(\frac{\nu-\nu_i}{250}\right)^4\right]\exp\left(-\left|\frac{\nu-\nu_i}{250}\right|\right) \tag{8}$$

and for *air*-broadening by

$$\chi' = 6.65 \exp\left[-\left(\frac{\nu-\nu_i}{75}\right)^2\right]. \tag{9}$$

These corrective functions are assumed to be temperature-independent. A polynomial fit of the H_2O partition function $Q(T)$ has been used to compute line intensities.[41]

In order to increase computational speed, the real absorption coefficient (before reordering) at a spectral location ν is split in three parts: (i) the far wing contribution of the lines centered at ν_i, such that $|\nu - \nu_i|$ is greater than 25 cm^{-1}; (ii) the contribution of lines characterized by $|\nu - \nu_i|$ between 3 and 25 cm^{-1}; (iii) the contribution of the line center region with $|\nu - \nu_i|$ smaller than 3 cm^{-1}. There are different reasons for this decomposition. The pressure dependence of wing contributions ($|\nu - \nu_i| > 3$ cm^{-1}) is well known; the volume absorption coefficient given in cm^{-1} is proportional to the square of the pressure. This contribution may be calculated at relatively low spectral resolutions. The cut-off at 25 cm^{-1} is due to the very different behavior of the functions $\chi(\nu - \nu_i)$ related to self-broadening and to *air*-broadening of H_2O lines beyond 25 cm^{-1}, while these functions are practically identical below 25 cm^{-1}.[8] The contributions (ii) and (iii) to the quantity $k^j_{gm}/(x_{H_2O}p)$, where x_{H_2O} is the water vapor molar fraction and p the total pressure, depend on the molar fractions only through the Lorentz half-widths. Then, the same procedure as that used in the case of Lorentz lines may be applied.[36] The model parameters for any mixture composition at a given pressure are deduced from those related to a reference mixture at an effective pressure, which leads to the same mean collisional half-width as under actual conditions.

This procedure cannot be applied for the contribution (i). Fortunately, this contribution has no spectral structure inside each spectral range $\Delta\nu$ and can be characterized by a constant mean absorption coefficient $\kappa^{>25}_{\Delta\nu}$. In practice, this coefficient is calculated by using a simple weighting of the coefficients calculated for pure H_2O and for H_2O infinitely diluted in air. It is given for a spectral narrow-band by

$$\kappa^{>25}_{\Delta\nu} = \frac{x_{H_2O}p}{kT}\left[(1 - x_{H_2O})\frac{p}{p_s}\bar{C}^{\Delta\nu}_{air} + x_{H_2O}\frac{p}{p_s}\bar{C}^{\Delta\nu}_{H_2O}\right], \tag{10}$$

where p_s is equal to 1 atm and $\bar{C}^{\Delta\nu}_j$ ($j = H_2O$ or *air*) is given by

$$\bar{C}^{\Delta\nu}_j = \frac{1}{\Delta\nu}\sum_{\substack{\text{lines } i \\ |\nu-\nu_i|>25}}\int_{\Delta\nu}\frac{\gamma^i_{L,j}(p_s,T)S_i(T)}{\pi(\nu-\nu_i)^2}\chi_j(\nu-\nu_i,T)\,d\nu. \tag{11}$$

The qualitites $\bar{C}^{\Delta\nu}_{air}(T)$ and $\bar{C}^{\Delta\nu}_{H_2O}(T)$ have been calculated with a 5 cm^{-1} resolution by using all lines of the approximate data base which are centered less than 1000 cm^{-1} away from the calculation point.

The contribution (ii) has been calculated for a reference H_2O–air mixture with 1 cm^{-1} resolution and linear interpolations are used to add it in a correlated manner to the contribution (iii), which is calculated with a maximum resolution of 10^{-3} cm^{-1}. The absorption coefficient is then reordered and its values at the quadrature points are stored.

For the 10 point quadrature and ckfg model, the reduced parameters corresponding to contributions (ii) and (iii)

$$k^{*j}_{gm} = \frac{k^j_{gm}TQ(T)}{x_{H_2O}p} \tag{12}$$

have been calculated for discrete temperature and pressure values in the ranges [180–2500 K] and [10^{-2}–6 atm]. Analytical functions of the form

$$f(T,p) = \exp\left(-\frac{E}{T}\right)\sum_{i=0}^{3}\sum_{j=0}^{i}a_{i,j}T^ip^j \tag{13}$$

have then been adjusted to analytically represent the variations of the reduced parameter k_{gm}^{*j} for each quadrature point m and fictitious gas j. The parameter E is a representative value of line lower level energies for the considered fictitious gas. The error generated by the use of the adjusted parameters in the calculation of the absorption coefficient averaged over each spectral range $\Delta\nu$ has been calculated for each set of temperature and pressure conditions used for the adjustment. The mean arithmetic value of these errors is 4.1% and their quadratic mean value is 9.0%. These errors are quite large since the adjustments have been carried out for wide ranges of temperature and pressure.

2.2. SNB models

The accuracy of ck and ckfg models must be compared to that of commonly used statistical narrow-band (SNB) models. In this section, we present the SNB models chosen for comparison and the corresponding parameters. We consider only random SNB models with the exponential tailed inverse distribution of line intensities,[12] since they are more accurate in the Lorentz regime.[16] In addition, we do not consider the approaches of Fels[24] and Zhu[25] which have not been formulated with this distribution function and which lead to an accuracy similar to that of the models combining the Doppler $\bar{W}_D$ and the Lorentz $\bar{W}_L$ black line equivalent widths.

The equivalent width averaged over the lines contained within the interval $\Delta\nu$ in the case of Voigt profiles is approximated by

$$\bar{W}_V = \sqrt{\bar{W}_L^2 + \bar{W}_D^2 - \left[\frac{\bar{W}_L \bar{W}_D}{\bar{k}xpl}\right]^2}. \tag{14}$$

in the formulation of Ref. 28, and by

$$\bar{W}_V = \bar{k}xpl\sqrt{1-\Omega^{-1/2}} \tag{15}$$

$$\Omega = \left[1-\left(\frac{\bar{W}_L}{\bar{k}xpl}\right)^2\right]^{-2} + \left[1-\left(\frac{\bar{W}_D}{\bar{k}xpl}\right)^2\right]^{-2} - 1. \tag{16}$$

in Ref. 29. In these expressions, $\bar{k}$ is the mean absorption coefficient per unit partial pressure, and $\bar{W}_L$ and $\bar{W}_D$ designate the equivalent widths averaged in the sense of the Malkmus line intensity distribution function.[12] $\bar{W}_L$ and $\bar{W}_D$ are given in Ref. 12, Eq. (28) and Ref. 20, Eq. (36), respectively, as functions of an effective Lorentz half-width, γ_{0L}, assigned to all the lines contained within $\Delta\nu$ and of the two parameters S_m and R of the intensity distribution function. These last two parameters may be seen as the maximum line intensity and the maximum to minimum line intensity ratio, respectively. The identification of the transmissivity expressions in the weak and the strong absorption limits leads to

$$S_m = \pi\bar{k}\bar{\delta}\frac{\gamma_{0L}}{\bar{\gamma}_L} \tag{17}$$

$$\ln R = \pi\frac{\gamma_{0L}}{\bar{\gamma}_L}\frac{\bar{\delta}}{\bar{\delta}}, \tag{18}$$

where $\bar{k}$, $\bar{\delta}$ and $\bar{\gamma}_L$ are the usual Lorentz band model parameters whose expressions are given, for instance, in Ref. 16, Eq. (6) and δ is the mean line spacing. Equation (28) of Ref. 12 and Eqs. (17) and (18) lead, in the limit of high R values, to an expression of $\bar{W}_L/\delta$ as function of only $\bar{k}$ and $\bar{\gamma}_L/\bar{\delta}$. The parameters $\bar{k}$ and $1/\bar{\delta}$ used here to calculate $\bar{W}_L/\delta$ have been adjusted to fit the line-by-line calculations in a previous paper[38] and tabulated vs temperature and wave-number. For Doppler profiles, a similar identification in the weak and strong absorption limit does not yield simple analytical expressions. Nevertheless, $\bar{W}_D/\delta$ can be calculated from $\bar{k}$ and the Lorentz parameter $1/\bar{\delta}$. We assume that γ_{0L} is equal to the mean Lorentz half-width $\bar{\gamma}_L$ and use the same distribution of line intensities with the parameters S_m and R identified in the Lorentz regime. Introducing Eqs. (17) and (18) in Eq. (36) of Ref. 20 leads to

$$\frac{\bar{W}_D}{\delta} = \bar{\beta}_D H\left(\frac{\bar{k}xpl}{\bar{\beta}_D}\right) \tag{19}$$

with

$$\bar{\beta}_D = \frac{1}{\sqrt{\pi \ln 2}} \frac{\gamma_{0D}}{\delta} \tag{20}$$

and

$$H(y) = \frac{1}{\sqrt{\pi}} \int_{-\infty}^{\infty} \ln(1 + y\, e^{-\xi^2})\, d\xi. \tag{21}$$

The Doppler half-width at half-maximum γ_{0D} is assumed constant over the interval $\Delta\nu$. In expressions (19) and (20), we use the Lorentz parameters calculated in Ref. 38 from their definitions, rather than those adjusted to line by line calculations.

Two approximations have been used to calculate $\bar{W}_L/\delta$ and $\bar{W}_D/\delta$ in the case of nonuniform columns: (i) the Curtis–Godson approximation as given in Ref. 21, Eqs. (10a, (10b) and (10c,) and (ii) the Lindquist–Simmons intuitive approximation as given in Ref. 22, Eq. (9) for Lorentz profiles and in Ref. 22, Eq. (11) for Doppler profiles.

3. MODEL COMPARISONS AND DISCUSSION

In this section, we compare results obtained from the ck and ckfg models with those of the line-by-line approach and SNB models. The considered models are:

(i) The ck model using 17 (ck17) or 10 (ck10) quadrature points.
(ii) The ckfg model using 17 (ckfg17) or 10 (ckfg10) quadrature points. For the ckfg10 model, we use both the reordered absorption coefficient values directly obtained from line-by-line calculations and those calculated from the adjustment given by Eq. (13).
(iii) The SNB model using the approximation of Crisp et al Eq. (14), associated with the Curtis–Godson (CG) or with the Lindquist–Simmons intuitive (LS) approximation for nonhomogeneous media.
(iv) The SNB model using the approximation of Ludwig et al Eq. (15), associated with the same nonhomogeneous approximations as for (iii) above.

The same spectroscopic data base is used to perform line-by-line calculations and to generate model parameters. Line-by-line calculations and the deviations of other models from these calculations are shown in the following figures. We will consider successively the case of homogeneous media, the case of isothermal but nonisobaric media, and finally the csae of isobaric and nonisothermal media.

Figure 4 shows the emissivity of a homogeneous 5 m long column of a H_2O–air mixture with $x_{H_2O} = 0.1$, at 2100 K and 0.1 atm. Under these conditions, the equivalent Doppler and Lorentz widths are of the same order. The ck17 and ckfg17 models introduce less than 4% relative error in the emissivity while the use of Eqs. (14) and (15) leads to overestimations of approx. 15 and 20%, respectively. It is worth noticing that for this case, the ck10 model is as accurate as the ck17 and the ckfg17 models, while the ckfg10 model leads to a maximum error of about 10%. In fact, the 10 point quadrature is sufficient to integrate the high resolution reordered emissivity of the real gas, but not the emissivities of the fictitious gases characterized by steeper variations, since the spectrum of each fictitious gas contains fewer lines than that of the real gas.

The emission spectrum near 5500 cm^{-1} of another homogeneous 50 m long column of a H_2O–air mixture with $x_{H_2O} = 0.1$, at 2000 K and 0.15 atm is plotted in Fig. 5. The ckfg10 model, used with the parameters adjusted by Eq. (13), agrees well with line-by-line calculations. This agreement shows the typical quality of the adjustment, even if it has been carried out for wide ranges of pressure and temperature. The results of the ckfg10 model in Fig. 5 are more accurate than those shown in Fig. 4, since the Doppler widths near 5500 cm^{-1} are larger than those near 1500 cm^{-1}. The accuracy of the SNB models in Fig. 5 is of the same order as in Fig. 4.

In Fig. 6, we consider the transmissivity of the set of two adjacent columns at the same temperature (2100 K) and composition (10% H_2O), but at different pressures. The first column is 5 cm long, at 6 atm, while the second is 5 m long, at 0.1 atm. Absorption lines are then characterized

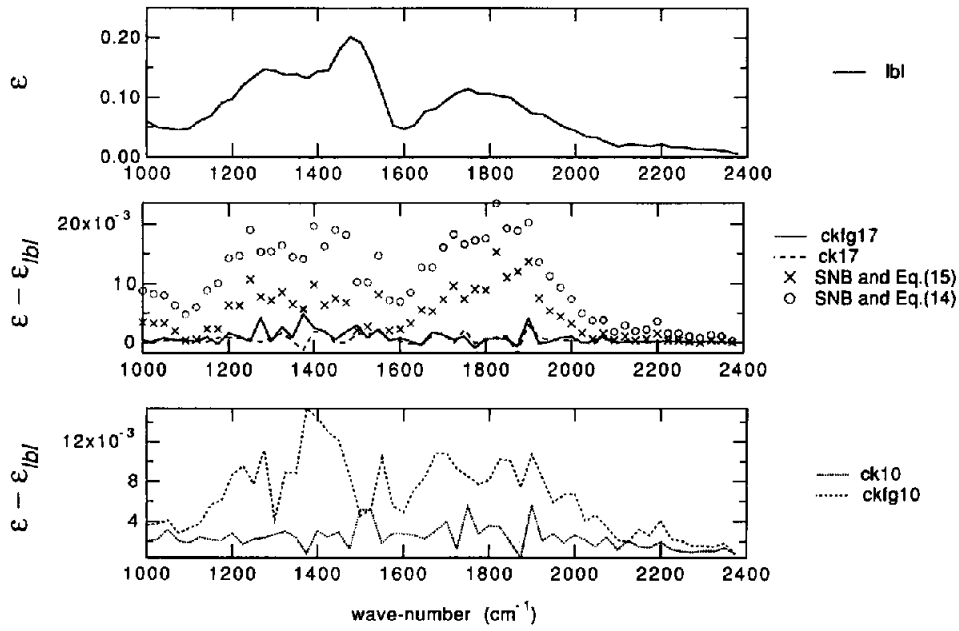

Fig. 4. Emissivities averaged over 25 cm^{-1} of a homogeneous H_2O–air mixture computed from line-by-line approach and from various models: $l = 5$ m, T = 2100 K, $p = 0.1$ atm, and $x_{H_2O} = 0.1$.

by a Lorentz profile for the first column and a Voigt profile (with $W_L \sim W_D$) for the second column. ckfg results are not shown in this figure, since this model is intended to account for highly variable temperature within a pathlength. Results from the ck and SNB-LS models agree well with line-by-line calculations. The Curtis–Godson approximation, however, may introduce a relative error greater than 30% in the emissivity. As shown by Young in the case of Lorentz lines,[19] the CG approximation is not accurate in the case of strong variations in line widths.

We finally consider two configurations related to long-range sensing. Figures 7 and 8 show the quantity $\overline{\epsilon_{1\nu}\tau_{2\nu}}^{\Delta\nu}$, where $\epsilon_{1\nu}$ designates the spectral emissivity of a 5 m long homogeneous column ($T = 2100$ K, $p = 0.1$ atm, $x_{H_2O} = 0.1$) and $\tau_{2\nu}$ is the transmissivity of the cold column ($T = 300$ K, $p = 0.1$ atm, $x_{H_2O} = 0.01$) which is 200 m long in the case of Fig. 7 and 10 km long in the case of Fig. 8. In practice, as required by the ckfg and SNB models, the calculated quantity is $\overline{\tau_{1\nu}}^{\Delta\nu} - \overline{\tau_{1\nu}\tau_{2\nu}}^{\Delta\nu}$.

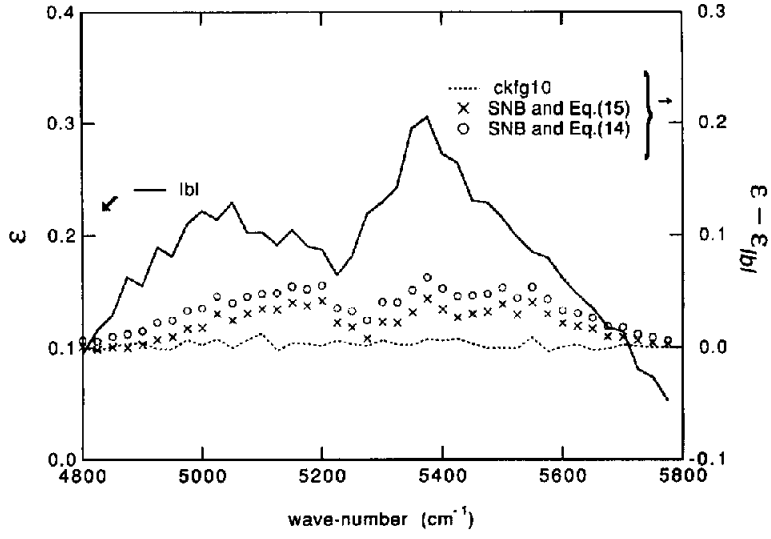

Fig. 5. Emissivities of a homogeneous H_2O–air column of length $l = 50$ m, temperature $T = 2000$ K, $x_{H_2O} = 0.1$ and pressure $p = 0.15$ atm, ckfg model is used with the adjusted parameters.

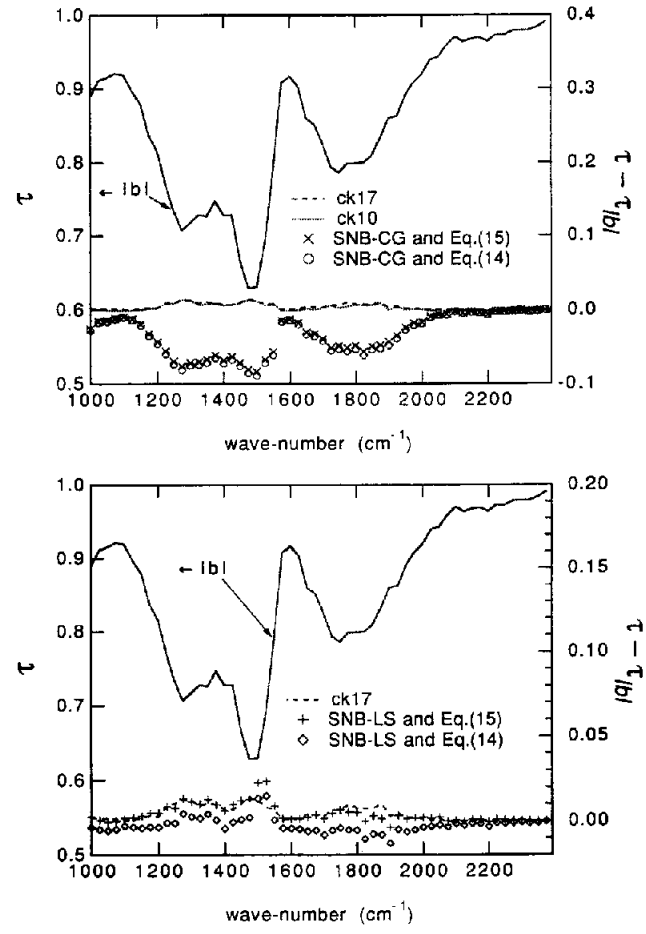

Fig. 6. Transmissivities averaged over 25 cm^{-1} of a set of two adjacent columns at the same temperature (2100 K) and composition (10% H_2O) but at different pressures; $p_1 = 6$ atm, $l_1 = 5$ cm, $p_2 = 0.1$ atm, $l_2 = 5$ m.

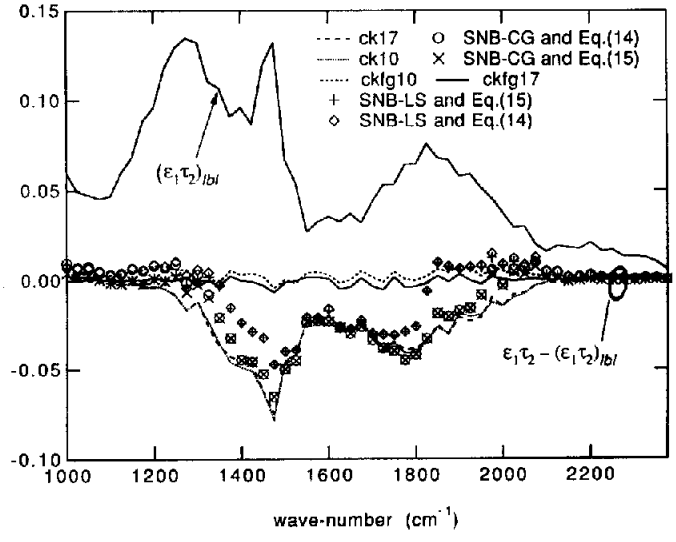

Fig. 7. Dimensionless radiation intensity emitted by a hot column ($T = 2100$ K, $p = 0.1$ atm, $x_{H_2O} = 0.1$, $l = 5$ m) and transmitted through a cold column ($T = 300$ K, $p = 0.1$ atm, $x_{H_2O} = 0.01$, $l = 200$ m). The intensity is divided by the Planck's function at 2100 K.

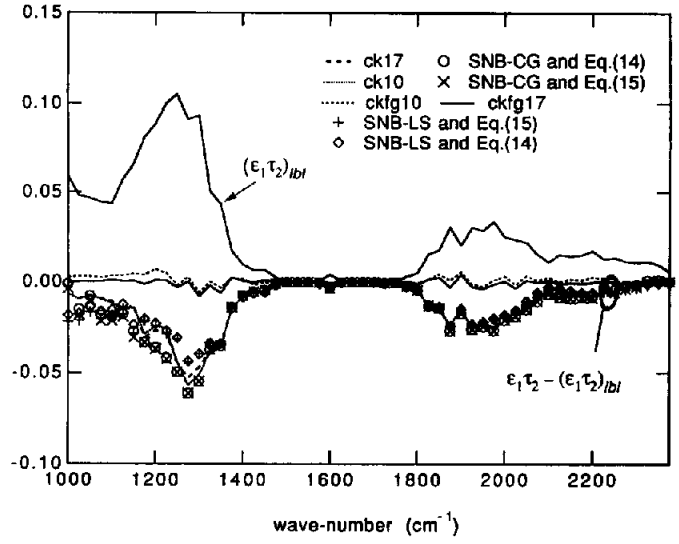

Fig. 8. Same as in Fig. 7 except the length of the cold column; $l = 10$ km.

From Figs. 7 and 8, it is observed that the ckfg10 and ckfg17 models yield very accurate results. It may be noted, however, that the ck and SNB models significantly underestimate the emitted and transmitted intensities (up to 80%).

It is worth noticing that the ck and SNB models, with CG or with LS approximations, lead to a similar underestimation of the emitted intensities for highly nonisothermal media. In fact, Young[19] has shown that the CG and LS approximations are based on the assumption that the intensities and widths of all the lines inside the spectral range have the same functional form vs temperature and partial pressures. On the other hand, the correlated-k approach gives exact results under the similarity hypothesis, i.e., when the absorption coefficient may be factorized as a product of a function of the wave-number and a function of temperature and partial pressures. These similar conditions, even if they are sufficient but not necessary, can explain the very similar results obtained with the SNB and ck approximations.

To conclude the above comparisons in the Voigt regime, it appears that: (i) for a homogeneous medium, the ck and ckfg models lead to a good agreement with LBL results and are more accurate than SNB models combining Doppler and Lorentz equivalent widths; however, the ckfg model is not interesting in this case: (ii) for nonisobaric media with small temperature variations, results from the ck approach agree well with LBL calculations and are more accurate than the results of the SNB model with the CG approximation; the SNB model with the LS approximation leads to the same accuracy as the ck model; (iii) for highly nonisothermal columns, including long cold paths, only ckfg results agree well with LBL calculations. The idea of separating molecular lines by lower level energies, which is used to build the ckfg model, significantly improves the accuracy of the ck method.

Acknowledgements—This work has been supported in part by the Société Nationale d'Etudes et de Construction de Moteurs d'Aviation. Computation facilities were made available to us by l'Institut de Développment et des Ressources en Informatique Scientifique (IDRIS).

REFERENCES

1. R. H. Dicke, *Phys. Rev.* **89,** 472 (1953).
2. L. Galatry, *Phys. Rev.* **122,** 1218 (1961).
3. R. M. Goody and Y. L. Yung, *Atmospheric Radiation*, Oxford University Press, New York (1989).
4. Q. Ma and R. H. Tipping, *J. Chem. Phys.* **93,** 7066 (1990).
5. P. W. Rosenkranz, *J. Chem. Phys.* **83,** 6139 (1985).
6. S. A. Clough, R. W. Davies, and R. H. Tipping. *Spectral Line Shapes.* Vol. 2, pp. 553–568, Walter de Gruyter, Berlin (1983).
7. J. M. Hartmann, M. Y. Perrin, Q. Ma, and R. H. Tipping, *JQSRT* **49,** 675 (1993).
8. S. A. Clough, F. X. Kneizys, and R. W. Davies, *Atmos. Res.* **23,** 229 (1989).

9. D. E. Burch, Continuum absorption by H_2O. AFGL-TR-81-0300 (1981).
10. D. E. Burch and R. L. Alt, Continuum absorption in the 700–1200 cm^{-1} and 2400–2800 cm^{-1} windows. AFGL-TR-84-0128 (1984).
11. D. E. Burch, Absorption by H_2O in narrow windows between 3000–4200 cm ^{1}. AFGL-TR-85-0036 (1985).
12. W. Malkmus, *J. Opt. Soc. Am.* **57,** 323 (1967).
13. W. M. Elsasser, *Phys. Rev.* **54,** 126 (1938).
14. S. J. Young, *JQSRT* **18,** 29 (1977).
15. L. S. Bernstein, D. C. Robertson, and J. A. Conant. *JQSRT* **23,** 169 (1980).
16. A. Soufiani, J. M. Hartmann, and J. Taine, *JQSRT* **33,** 243 (1985).
17. W. J. Phillips, *JQSRT* **43,** 13 (1990).
18. W. J. Phillips, *JQSRT* **48,** 91 (1992).
19. S. J. Young, *JQSRT* **18,** 1 (1977).
20. W. Malkmus, *J. Opt. Soc. Am.* **58,** 1214 (1968).
21. S. J. Young, *JQSRT* **15,** 483 (1975).
22. S. J. Young, *JQSRT* **15,** 1137 (1975).
23. S. A. Golden, *JQSRT* **9,** 1067 (1969).
24. S. B. Fels, *Appl. Opt.* **18,** 2634 (1979).
25. X. Zhu, *JQSRT* **39,** 421 (1988).
26. C. Gille and G. Ellingson, *Appl. Opt.* **7,** 471 (1968).
27. C. D. Rodgers and A. P. Williams, *JQSRT* **14,** 319 (1974).
28. D. Crisp, S. B. Fels, and M. D. Schwarzkopf, *J. Geophys. Res.* **91,** 11851 (1986).
29. C. B. Ludwig, W. Malkmus, J. E. Reardon, and J. A. L. Thomson, *Handbook of Infrared Radiation from Combustion Gases NASA SP*-3080, National Aeronautics and Space Administration, Washington, DC (1973).
30. J. M. Hartmann, J. P. Bouanich, C. Boulet, and M. Sergent, *J. Phys. II* **1,** 739 (1991).
31. A. Arking and K. Grossman, *J. Atmos. Sci.* **29,** (1972).
32. G. A. Domoto, *JQSRT* **14,** 935 (1974).
33. M. D. Chou and A. Arking, *J. Atmos. Sci.* **38,** 798 (1981).
34. R. Goody, R. West, L. Chen, and D. Crisp, *JQSRT* **42,** 539 (1989).
35. A. A. Lacis and V. Oinas, *J. Geophys. Res.* **96,** 9027 (1991).
36. Ph. Rivière, A. Soufiani, and J. Taine, *JQSRT* **48,** 187 (1992).
37. R. Levi Di Leon and J. Taine, *Revue Phys. Appl.* **21,** 825 (1986).
38. Ph. Rivière, S. Langlois, A. Soufiani, and J. Taine, *JQSRT* **53,** 221–234 (1995).
39. C. Delaye, J. M. Hartmann, and J. Taine, *Appl. Opt.* **28,** (1989).
40. S. R. Drayson, *JQSRT* **16,** 611 (1976).
41. R. R. Ganache, private communication.